Entropy **2014**, *16*, 6116-6132; doi:10.3390/e16116116

OPEN ACCESS

entropy

ISSN 1099-4300

www.mdpi.com/journal/entropy

Article

Entropy Generation during Turbulent Flow of Zirconia-water and Other Nanofluids in a Square Cross Section Tube with a Constant Heat Flux

Hooman Yarmand [1,*], Goodarz Ahmadi [2], Samira Gharehkhani [1], Salim Newaz Kazi [1], Mohammad Reza Safaei [1,†], Maryam Sadat Alehashem [3] and Abu Bakar Mahat [1]

[1] Department of Mechanical Engineering, Faculty of Engineering, University of Malaya, Kuala Lumpur 50603, Malaysia; E-Mails: s_gharahkhani_248@yahoo.com (S.G.); salimnewaz@um.edu.my or salimnewaz@yahoo.com (S.N.K.); cfd_safaiy@yahoo.com(M.R.S.); ir_abakar@um.edu.my (A.B.M.)

[2] Department of Mechanical and Aeronautical Engineering, Clarkson University, Potsdam, NY 13699, USA; E-Mail: gahmadi@clarkson.edu

[3] Department of Chemistry, Faculty of Science, University of Malaya, Kuala Lumpur 50603, Malaysia; E-Mail: maryam.alehashem@yahoo.com

[†] Current address: Young Researchers and Elite Club, Mashhad Branch, Islamic Azad University, Mashhad, Iran

* Author to whom correspondence should be addressed; E-Mail: hooman_yarmand@yahoo.com; Tel.: +(603)-7967-4582; Fax: +(603)-7967-5317.

External Editor: Kevin H. Knuth

Received: 8 July 2014; in revised form: 11 August 2014 / Accepted: 6 November 2014 / Published: 19 November 2014

Abstract: The entropy generation based on the second law of thermodynamics is investigated for turbulent forced convection flow of ZrO_2-water nanofluid through a square pipe with constant wall heat flux. Effects of different particle concentrations, inlet conditions and particle sizes on entropy generation of ZrO_2-water nanofluid are studied. Contributions from frictional and thermal entropy generations are investigated, and the optimal working condition is analyzed. The results show that the optimal volume concentration of nanoparticles to minimize the entropy generation increases when the Reynolds number decreases. It was also found that the thermal entropy generation increases with the increase of nanoparticle

size whereas the frictional entropy generation decreases. Finally, the entropy generation of ZrO_2-water was compared with that from other nanofluids (including Al_2O_3, SiO_2 and CuO nanoparticles in water). The results showed that the SiO_2 provided the highest entropy generation.

Keywords: entropy generation, nanofluid, turbulent flow

1. Introduction

The idea of using nanoparticles in fluids is not quite new. In fact, about one hundred years ago Maxwell [1] found that the thermal conductivity of a suspension of nanoparticles increased compared to that of the base fluid. However, the terminology of "nanofluids" was first introduced in 1995 by Choi [2] for a suspension of nanoparticles in base fluids. Nanoparticles could be silica, polymers, metal dioxides, metals and carbon nanotubes. Oil, water and ethylene glycol are the common base fluids. In many cases the nanofluids have higher thermal conductivity compared to that of the base fluid; consequently, the nanofluids have more desirable heat transfer properties. Nowadays many researchers are studying the potential use of nanofluids in a variety of engineering equipment to improve the energy efficiency and to enhance the system's thermal performance. Solar collectors [3], car radiators, chillers, boilers, cooling and heating systems in buildings, and micro-channel and heat pipes are just a few examples [4–15].

Kulkarni *et al.* [16] described the use of nanofluids to retard the decrease of cogeneration efficiency. The thermal conductivity of Cu-water nanofluids produced by a chemical reduction process was assessed by Liu *et al.* [17]. Haghshenas *et al.* [18] studied numerically the efficiency of laminar convective heat transfer to nanofluids. Mahmoudi *et al.* [19] simulated a nanofluid cooling system of natural convection process. Yoo *et al.* [20] and Xie *et al.* [21] outlined the methods of preparation and stability and the applications of nanofluids in the fields of energy conversion, mechanical engineering, and biomedical engineering. Maïga *et al.* [22] studied the hydrodynamic and thermal behavior of turbulent flows in a tube using an Al_2O_3 nanoparticle suspension at various concentrations and constant heat flux boundary conditions, and they reported enhanced thermal conductivity of the Al_2O_3 nanofluids. Vajjha *et al.* [23] investigated experimentally the forced convective heat transfer of nanofluids comprised of aluminum oxide, copper oxide and silicon dioxide dispersed in ethylene glycol and water in the fully developed turbulent regime, and they suggested an experimental correlation for the corresponding Nusselt number for this class of nanofluids. Recently, using numerical methods Yarmand *et al.* [24] studied the heat transfer to four different nanofluids in a rectangular heated pipe under a turbulent flow regime subject to constant heat flux boundary conditions. They found that the effect of Reynolds number on heat transfer to a nanofluid is more important than the effect of the concentration of nanoparticles.

In the recent years, entropy analyses of nanofluids for finding the optimal working condition of engineering systems have been studied by several researchers [25,26]. The ratio of irreversibility of a thermal system was estimated by the corresponding entropy generation, and ways to decrease it to improve the working condition was analyzed. Oztop and Al-Salem [27] wrote a review article on entropy generation in mixed and natural convection heat transfer for thermal systems. Sahin [28] examined the

entropy generation for different cross-section geometries of ducts at a constant wall temperature. The entropy generation in nanofluid flow between co-rotating cylinders and the changes in the entropy generated in such systems (due to physical properties) have been studied by some researchers [29,30]. Ko *et al.* [31] found the ideal Reynolds number for laminar flows with different wall heat fluxes in a double sine duct. Leong *et al.* [32] analyzed entropy generation of an alumina-water nanofluid under turbulent flow regime in a circular pipe under constant wall temperature. They reported that the flow rate and the length of pipe significantly affect the total dimensionless entropy generation. The effect of dynamic viscosity on the entropy generation of a turbulent flow was reported by Bianco *et al.* [33]. Moghaddamai *et al.* [34,35] performed entropy analyses on laminar and turbulent flows in a circular tube under constant heat flux. They found that, for the turbulent flow of the Al_2O_3-water nanofluid, the addition of nanoparticles enhances heat transfer when the Reynolds number is less than 40,000. The difference between this work [34] and the results of [35] is the difference in methods for obtaining entropy generation results. Moghaddamai *et al.* [35] first measured the velocity and temperature fields, and then the entropy generation distribution was evaluated locally [3]. Bianco *et al.* [36] studied the entropy generation and heat transfer enhancement of the forced convection turbulent flow of Al_2O_3 in a square cross section pipe and found the optimal Reynolds number.

The presented literature survey shows that a second law analysis of the turbulent forced convection flow of ZrO_2-water nanofluids in a square cross sectional duct at constant heat flux has not yet been addressed. In the present work, the entropy generation of ZrO_2, CuO, SiO_2 and Al_2O_3 nanofluids in a square duct was studied using the using the approach of Bianco *et al.* [37]. The nanofluid flows were in a turbulent forced convection regime with a constant wall heat flux. The effects of different parameters including particle size, volume concentration and Reynolds number on the entropy generation of ZrO_2-water nanofluid were studied. Both the frictional and the thermal entropy generations were included in the analysis. In particular, the concentration of nanoparticles for the optimal working performance of ZrO_2-water nanofluids in terms of minimizing entropy generation under turbulent forced convection flow with a constant heat flux in a square cross section duct was evaluated and discussed. Finally the entropy generation of the ZrO_2-water mixture was compared with the other nanofluids.

2. Methodology

2.1. Thermophysical Properties of Nanofluid

In order to conduct a numerical analysis of a nanofluid flow and heat transfer, its effective thermophysical properties must be determined first. Generally the relevant properties are effective thermal conductivity (k_{eff}), effective dynamic viscosity, effective mass density (ρ_{eff}) and effective specific heat (C_{peff}). These effective properties are typically evaluated using the mixing theory. According to Das [38] the variation of viscosity and thermal conductivity of nanofluids with the temperature is negligible. Therefore, the thermophysical properties of nanofluids are evaluated at the average temperature for different working conditions.

The density of a nanofluid, ρ_{nf}, is given as [39]:

$$\rho_{nf} = (1 - \varphi)\rho_f + \varphi\rho_{np} \quad (1)$$

where ρ_f and ρ_{np} are, respectively, the mass densities of the base fluid and the solid nanoparticles.

The effective heat capacity of nanofluid at constant pressure $(\rho\, C_p)_{nf}$ is given as:

$$(\rho\, C_p)_{nf} = (1-\varphi)(\rho\, C_p)_f + \varphi\, (\rho\, C_p)_{np} \tag{2}$$

where $(\rho\, C_p)_f$ and $(\rho\, C_p)_{np}$ are, respectively, the heat capacities of the base fluid and the solid nanoparticles.

The effective viscosity (μ_{eff}) is obtained using the empirical correlation suggested by Corcione [40]. That is:

$$\mu_{\text{eff}} = \mu_f \frac{1}{(1-34.87\,(d_p/d_f)^{-0.3} \times \varphi^{1.03})} \tag{3}$$

where:

$$d_f = \left[\frac{6M}{N\pi\rho_{fo}}\right] \tag{4}$$

Here M is the molecular weight of the base fluid; N is the Avogadro number = 6.022×10^{23} mol^{-1}; and ρ_{fo} is the mass density of the base fluid at temperature T_0 = 293 K.

By considering the Brownian motion of nanoparticles, the effective thermal conductivity can be obtained by using the empirical correlation provided in [3]. That is:

$$K_{\text{eff}} = k_{\text{static}} + k_{\text{Brownian}} \tag{5}$$

where:

$$k_{static} = k_f \left[\frac{(k_{np}+2k_f) - 2\emptyset\,(k_f - k_{np})}{(k_{np}+2\,k_f) + \emptyset(k_f + k_{np})}\right] \tag{6}$$

$$k_{\text{brownian}} = 5 \times 10^4\, \beta\emptyset\rho_f C_{p,f} \sqrt{\frac{kT}{2\rho_{np}.R_{np}}}\, f(T,\emptyset) \tag{7}$$

Here, R_{np} is the radius of the nanoparticle, and k = 1.3807×10^{-23} is the Boltzmann constant.

2.2. Governing Equations

Entropy generation for a nanofluid flowing through a square cross section is a combination of frictional and thermal entropy generation [26,41]. Accordingly:

$$S_{\text{gen,T}} = S_{\text{gen,t}} + S_{\text{gen,f}} \tag{8}$$

The thermal and frictional entropy generations for the unit length of the duct are given as (Bejan [26]):

$$S_{\text{gen,T}}\,(X) = \frac{\dot{q}.\Delta T(x)}{T^2} + \frac{m}{\rho T}\left(-\frac{dp}{dx}\right) \tag{9}$$

The first term in Equation (9) is the thermal entropy generation, and the second term is the frictional entropy generation. By integrating Equation (9), Bejan [26] obtained the following formula for a circular duct:

$$S_{\text{gen,T}} = \frac{q2.P.D.L}{Nu.k.T_{ave}} + \frac{2.m^3.f.L}{\rho.T_{ave}.D.A_c^2} \tag{10}$$

For a square cross sectional pipe, Bianco *et al.* [37] found:

$$S_{gen,T} = \frac{q2.\pi.D_h^2.L}{Nu.k.T_{ave}} + \frac{32.m^3.f.L}{\rho^2.T_{ave}.D_h^5.\pi} \quad (11)$$

where D_h and T_{ave} are given as:

$$D_h = \frac{4A_c}{P} \quad (12)$$

$$T_{ave} = \frac{T_{in} - T_{out}}{\ln\left(\frac{T_{in}}{T_{out}}\right)} \quad (13)$$

where A_c is the cross-sectional area and P is the perimeter.

Using an energy balance (first law) for the tube with a constant heat flux, T_{out} can be found as:

$$T_{out} = T_{in} + \frac{q \cdot A_s}{m \cdot C_p} \quad (14)$$

The corresponding thermal and frictional entropy generations are then, respectively, given as:

$$S_{gen,t} = \frac{q2.\pi.D_h^2.L}{Nu.k.T_{ave}} \quad (15)$$

$$S_{gen,f} = \frac{32.m^3.f.L}{\rho^2.T_{ave}.D_h^5.\pi} \quad (16)$$

where f is the friction factor and is given by [28,32]:

$$f = [0.79 \ln(\mathrm{Re}) - 1.64]^{-2} \quad (17)$$

The Nusselt number for turbulent forced convection of nanofluids may be obtained from the experimental study of Dittus and Boelter [42]. That is:

$$\mathrm{Nu} = 0.023.\ \mathrm{Re}^{0.8}.\mathrm{Pr}^{0.4} \quad (18)$$

where the Reynolds number is defined as:

$$\mathrm{Re} = \frac{\rho_{nf}.v.D_h}{\mu_{nf}} \quad (19)$$

To find the relative influences of thermal and frictional entropy generations on the total entropy generation, the non-dimensional Bejan number (Be) is used. The range of Be is from 0 to 1, where Be = 0 implies that all the entropy generation is due to friction and Be = 1 corresponds to the case where all the entropy generation is thermal. The Bejan number is defined as:

$$\mathrm{Be} = \frac{S_{gen,t}}{S_{gen,T}} \quad (20)$$

2.3. Description of the Problem

The second law analysis of a ZrO_2-water nanofluid in a square cross sectional pipe is investigated in this section. Schematic of the duct is shown in Figure 1. The length of the duct is 1 meter, and its hydraulic diameter is 0.01 m. The duct wall is at a constant heat flux of 50,000 W/m^2, and the inlet temperature is 300 K.

Figure 1. Schematic diagram of the square cross section duct.

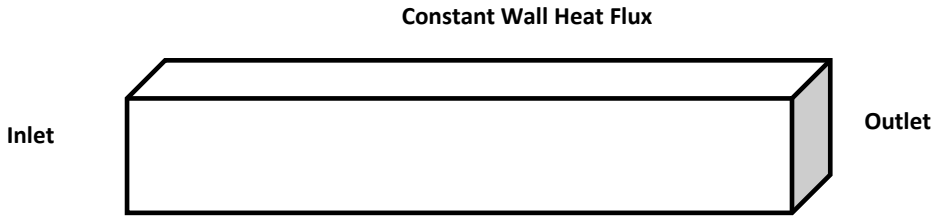

As a series of simulations are performed, where the flow Reynolds number is varied in the range of 50,000 to 70,000, the nanoparticle concentrations are varied in the range of 0% to 7%, and the nanoparticle diameters are varied in the range of 10 nm to 50 nm. While the ZrO_2-water nanofluids are of main concern, the effects of using different nanoparticle-water mixtures on the entropy generation are also investigated.

2.4. Validation

For validation the present model predictions are compared with the experimental data of Williams *et al.* [43] in Figure 2. Comparisons are done for three concentrations of 0.2%, 0.5% and 0.9% for ZrO_2-water nanofluids. This figure shows that there is a good agreement between the entropy productions estimated by the present model and the experimentally measured data. The average difference for the three concentrations shown is about 0.85%. This slight difference may be attributed to experimental error or the inaccuracies in the formula used for the effective thermal conductivity and/or effective viscosity of the ZrO_2-water mixtures.

Figure 2. Comparison of the predicted entropy generation with the experimental data of Williams *et al.* [43] for ZrO_2-water nanofluids.

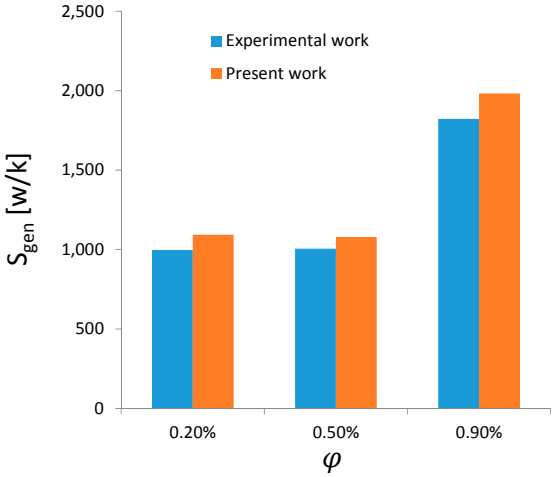

3. Results and Discussion

In this section the effects of nanoparticle concentration, Reynolds number, nanoparticle diameter and type of nanoparticle material on entropy generation are investigated. The ZrO_2-water nanofluid is used for studying the effect of variations in nanoparticle concentration, Reynolds number, and nanoparticle

diameter. For the case of studying the effect of nanoparticle material, the entropy generation for suspensions of Al_2O_3, ZrO_2, SiO_2 and CuO in water are evaluated and compared with each other.

3.1. Effects of Nanoparticle Concentration

Here the variations of thermal and frictional entropy generations with nanoparticle concentration are investigated. For the turbulent flow of ZrO_2-water nanofluids at Re = 60,000 in the square cross section duct with a wall heat flux of 50,000 w/m^2, Figure 3 shows the predicted variations of total entropy generation, as well as the thermal and frictional entropy generations with particle volume concentrations in the range of 0 to 7%. Here the diameter of the ZrO_2 particles is d_p = 20 nm. It is seen that the thermal entropy generation is dominant compared with the frictional entropy generation in this case. Furthermore, the thermal and frictional entropy generations have opposing trends of variation with increasing concentration of nanoparticles. That is, with the increase of nanoparticle concentration, the thermal entropy generation decreases while the frictional entropy generation increases. The decreasing trend of entropy generation may be justified by examining Equation (15), where the increase of the effective thermal conductivity and Nusselt number with the increase of particle concentration leads to a decrease in the thermal entropy generation. The frictional entropy generation, however, increases with particle concentration since the effective viscosity increases. Although with the increase of nanoparticle concentration both the viscosity and density of nanofluid increase, the increase of viscosity is far more than the increase of density which leads to an increase of the shear stress [36]. Thus, to maintain a constant Reynolds number, the velocity has to be increased. The increase of velocity (mass flow rate) has a direct effect on the increasing trend of frictional entropy generation at a constant Reynolds number.

Figure 3. Variation of thermal, frictional and total entropy generations with nanoparticle concentration in % for ZrO_2-water nanofluid with dp = 20 nm at Re = 60,000.

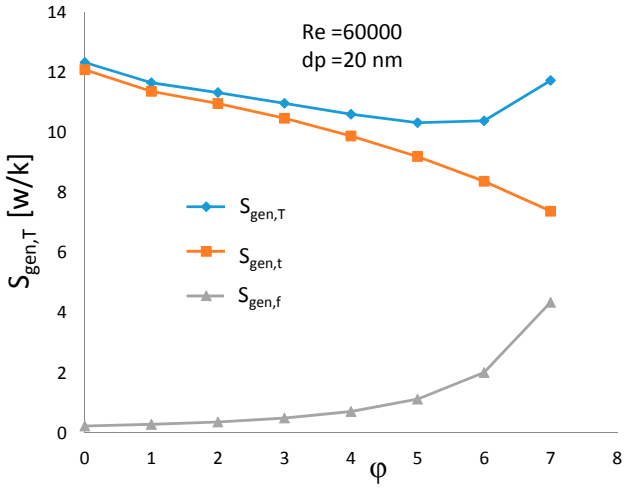

Due to the opposing trends of the thermal and frictional entropy generations with particle volume fraction, the total entropy generation gets a minimum value that can be seen in Figure 3. This figure suggests that the optimal working condition with minimum net entropy generation for the ZrO_2-water nanofluid at a constant Reynolds number flow in a square duct with a constant heat flux is at a nanoparticle concentration of about 5% to 6%.

3.2. Effects of Reynolds Number

In this section, the effects of the Reynolds number on the thermal and frictional entropy generations are studied. Figure 4 shows variations of thermal, frictional and total entropy generations, as well as the Bejan (Be) number *versus* nanoparticle concentrations at different Reynolds numbers (Re = 50,000, 60,000 and 70,000) at d_p = 20 nm.

Figure 4. Variations of (**a**) thermal entropy generation ($S_{gen,t}$); (**b**) frictional entropy generation ($S_{gen,f}$); (**c**) total entropy generations ($S_{gen,T}$) and (**d**) Bejan (Be) number for ZrO_2-water nanofluid at d_p = 20 nm with nanoparticle concentrations at different Reynolds numbers.

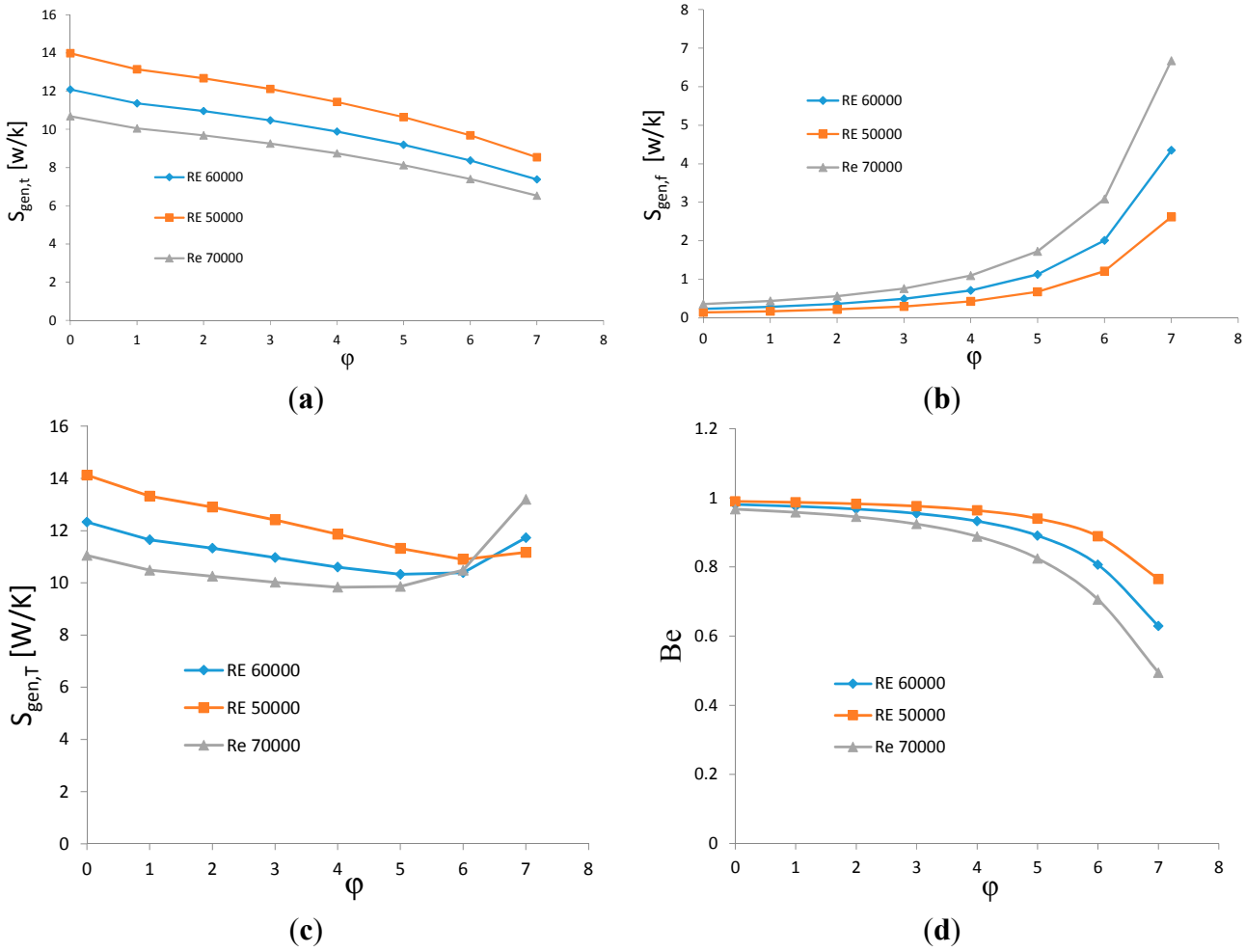

Figure 4a shows that the thermal entropy generation decreases with the increase of the Reynolds number. In contrast, Figure 4b shows that the frictional entropy generation increases with the increase of the Reynolds number. This trend is due to the fact that the Nusselt number increases with the increase of Reynolds number, as shown by Equation (18). The increase of Nusselt number implies that the thermal entropy generation as given by Equation (15) decreases. The increase of frictional entropy generation is due to the increase of the friction factor, as given by Equation (17), which increases with the increase in Reynolds number.

According to Figure 4b the frictional entropy generations for the three Reynolds numbers studied are quite low and roughly the same order for low solid volume concentrations (≤3%). As the concentration

of the nanoparticle increases, however, the differences become noticeable, and the flow with higher Reynolds number produces higher frictional entropy. Furthermore, the rate of change of the frictional entropy generation *versus* the nanoparticle concentration has a higher slope at the higher Reynolds number.

Figure 4c illustrates the variation of total entropy generation *versus* the nanoparticle concentration for different Reynolds numbers. As noted before, due to the decreasing and increasing trends of thermal and frictional entropy generations, the total entropy generation exhibits an optimum condition with minimum entropy generation. It is seen that the minimum entropy generation shifts to the lower concentration as Re increases. That is, the minimum entropy production occurs at about 6% to 7% for Re = 50,000, but shifts to about 5% to 6% for Re = 60,000. For Re = 70,000, the minimum total entropy production occurs at about 4% to 5% nanoparticle concentration. When Re increases, the frictional entropy generation becomes more significant and the total entropy generation increases; thus, the value of concentration which minimizes the total entropy generation reduces.

The variations of the Bejan number with particle concentration for different Re are shown in Figure 4d. This figure shows that the thermal entropy generation is dominant at lower particle concentrations, but the effect of frictional entropy generation increases at higher particle concentrations, particularly, at higher Reynolds numbers. At low Reynolds numbers, the entropy generation is dominated by the irreversibility of heat transfer, whereas with increasing values of Re and particle concentration, the entropy generation, due to friction losses, becomes more important.

3.3. Effect of Nanoparticle Diameter

In this section the effect of nanoparticle diameter on the thermal and frictional entropy generations is investigated. Figure 5 shows variations of thermal, frictional and total entropy generations, as well as, Bejan number *versus* particle concentration in the range of φ = 0% to 7% for different nanoparticle diameters (d_p = 10, 20, and 50 nm) at Reynold number = 60,000. Figure 5a shows that the thermal entropy generation increases as nanoparticle diameter increases. Teng *et al.* [44] and Kleinstreuer and Feng [45] among others have reported that the thermal conductivity of nanofluids decreases with an increase in nanoparticle size. Equation (15) for the thermal entropy production shows that the thermal entropy generation is inversely proportional to the thermal conductivity. As a result, an increase in particle size leads to an increase in thermal entropy generation. This fact is due to the enhancement of heat transfer due to the increase of thermal conductivity of nanofluids, which is inversely proportional to the nanoparticle size at the same volume concentration. This is because smaller particles have higher surface area for interaction with the liquid phase.

Figure 5b indicates that at a constant volume concentration and constant Reynolds number, the frictional entropy generation decreases with the increase of nanoparticle size. The decrease of frictional entropy generation is due to decreasing of the frictional losses which is associated with the decrease in mass flow rate. Equation (3) shows that the effective viscosity decreases as nanofluid particle size increases; therefore at a constant Re, the mass flow rate decreases and Equation (16) shows that the frictional entropy generation which is proportional to cube of mass flow rate decreases.

Figure 5c shows the variation of the total entropy generation *versus* the nanoparticle concentration for different nanoparticle diameters. Since the thermal and frictional entropy generations follow opposite

trends with increase of concentration and nanoparticle size, there is a critical concentration for the minimum total entropy production. Figure 5c shows the concentration for the minimum entropy generation varies significantly with the nanoparticle diameter. For 10 nm particles, there is a clear minimum value at the concentration of about 4%, and critical concentration shifts to about 5% to 6% for dp = 20 nm. For 50 nm particles, the total entropy production continues to decrease with the increase of concentration, indicating that the minimum entropy occurs at concentrations larger than 6%. Figure 5c also shows that the total entropy production for different size particles is only slightly different for concentrations less than 4% or 5% and follows the trend of thermal entropy production. For higher concentrations, when the frictional contribution becomes important, the differences become more noticeable.

Figure 5. Variations of (**a**) thermal entropy generation ($S_{gen,t}$); (**b**) frictional entropy generation ($S_{gen,f}$); (**c**) total entropy generations ($S_{gen,T}$) and (**d**) Bejan (Be) number *versus* nanoparticle concentrations at Re = 60,000 for different nanoparticle diameters of ZrO_2-water nanofluid.

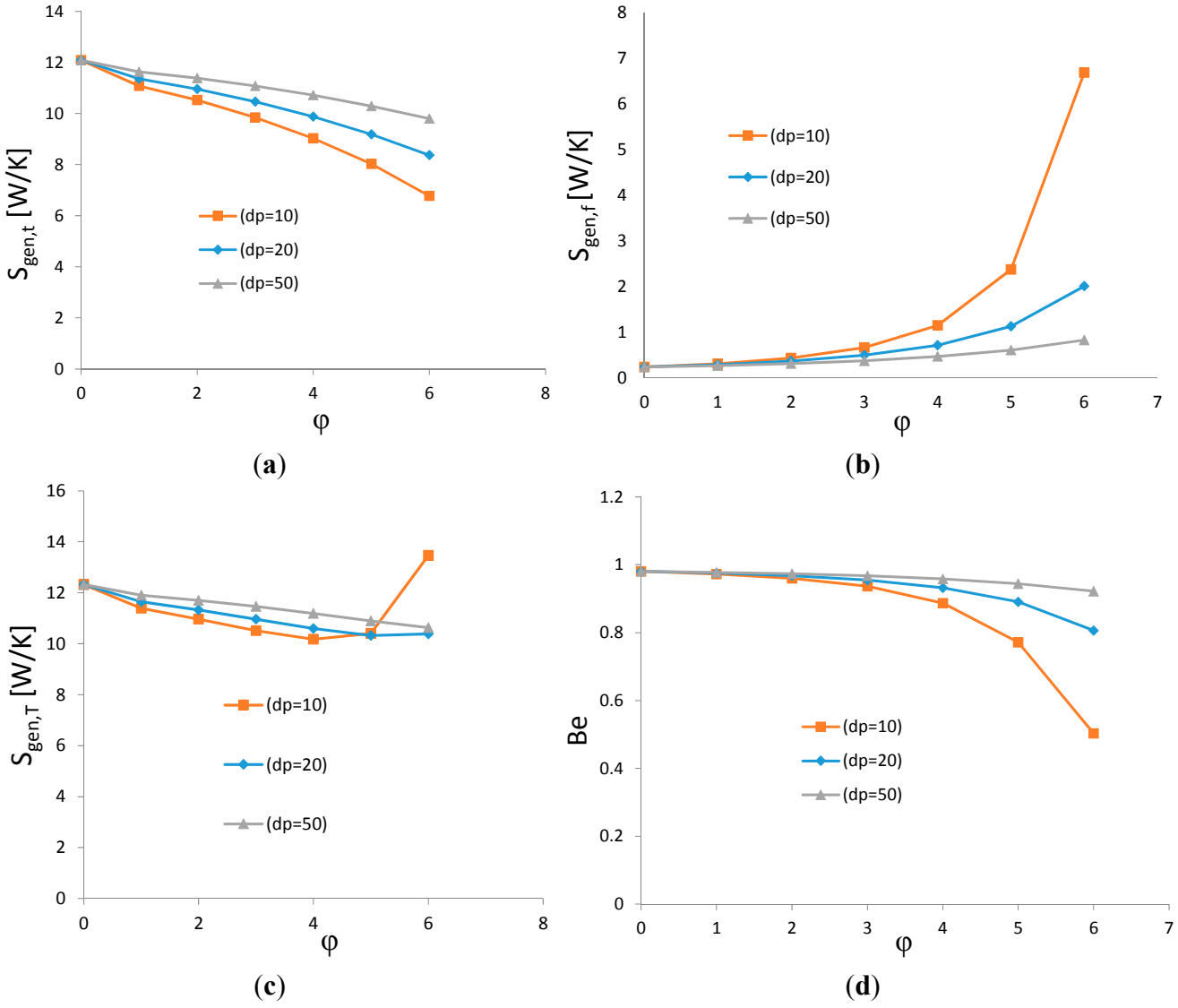

Variation of the Bejan number with concentrations for different nanoparticle sizes is shown in Figure 5d. It is seen that Be is about 1 and the effect of particle size is negligible for concentrations less than 3%, indicating that the entropy generation is mainly thermal. For larger concentrations, the effect of frictional entropy generation on Bejan number becomes more noticeable particularly for 10 nm particles.

In summary, Figures 5a–d reveal that the total entropy production of ZrO_2-water nanofluids is dominated by the thermal generation at all concentrations, particularly for larger diameter nanoparticles. It can be seen that when d_p is smaller and concentration is higher, the frictional entropy generation starts to become more significant.

3.4. Effect of Different Nanoparticles

In this section, entropy generations for water-based nanofluids with different nanoparticle materials are studied. Figure 6 compares the variations of entropy generation of different nanofluids *versus* solid volume concentration. Nanofluids with four different nanoparticle materials (Al_2O_3, ZrO_2, SiO_2 and CuO) are studied. For all nanofluids, the same inlet condition with Re = 60,000 and the same nanoparticle size dp = 20 nm are used in the analysis.

The variations of thermal entropy production of different nanofluids are shown in Figure 6a. It is seen that the thermal entropy productions for different nanofluids decrease with increase of concentration. ZrO_2 nanofluid typically leads to the highest thermal entropy generation, and Al_2O_3 nanofluids generate the lowest thermal entropy among the nanofluids studied. This is perhaps due to the fact that Al_2O_3 has the highest thermal conductivity compared to the other nanoparticles studied. Equation (15) shows that the thermal entropy generation is inversely proportional to the effective thermal conductivity. In other words, the Al_2O_3 nanofluids have better heat transfer characteristics compared to the other nanoparticles used in the present study and thus lead to lower thermal entropy generation.

Figure 6b compares the frictional entropy generation for different nanofluids. It is seen that the frictional entropy productions of different nanofluids increase with concentration but are roughly the same at the low solid volume fractions. For concentrations higher than 4%, the trend of increase with volume fraction becomes sharper, and the differences in frictional entropy productions become more significant. Figure 6b also shows that the SiO_2-water nanofluid has the highest $S_{gen,f}$ among the nanofluids considered at the same Reynolds number and concentration. This is because SiO_2 has the highest density, and Equation (16) shows that the frictional entropy generation is roughly linearly proportional to the effective density of the nanofluid. (Equation (16) shows that $S_{gen,f}$ is proportional to the cube of mass flow rate divided by density square). In summary, the nanofluid with higher density generates more friction loses which leads to higher friction entropy generation.

Variations of the total entropy production with solid volume fraction for different nanofluids are shown in Figure 6c. Since concentration range is extended to 7%, the v-shape variation of total entropy production can be clearly seen in the figure. This figure shows that all nanofluids studied have an optimum concentration for minimum entropy production at the concentration range of 5% to 6%. As mentioned before, for ZrO_2-water nanofluid, the optimal working condition is at a solid volume fraction of about 5% to 6%. The SiO_2-water nanofluid generates the highest total entropy production, with its minimum value at a concentration of 5%. The optimal working condition for the Al_2O_3-water nanofluid,

which has the lowest total entropy generation, is also at a concentration of 5%. The minimum entropy production of CuO-water nanofluid occurs at about 6% concentration. Figure 6c shows that the effect of frictional entropy generation becomes markedly significant at higher concentrations.

Figure 6d compares the variation of Bejan number as a function of volume concentration for different nanofluids. It is seen that the trend of variation of Bejan number is roughly the same for all the nanofluids studied. Only at concentrations larger than 5%, do the differences become noticeable. It is seen that the ZrO_2-water nanofluid leads to the highest value of Bejan number, while SiO_2-water nanofluid leads to the lowest values.

Figure 6. Variations of (**a**) thermal entropy generation ($S_{gen,t}$); (**b**) frictional entropy generation ($S_{gen,f}$); (**c**) total entropy generations ($S_{gen,T}$) and (**d**) Bejan (Be) number *versus* nanoparticle concentrations for different types of nanoparticles.

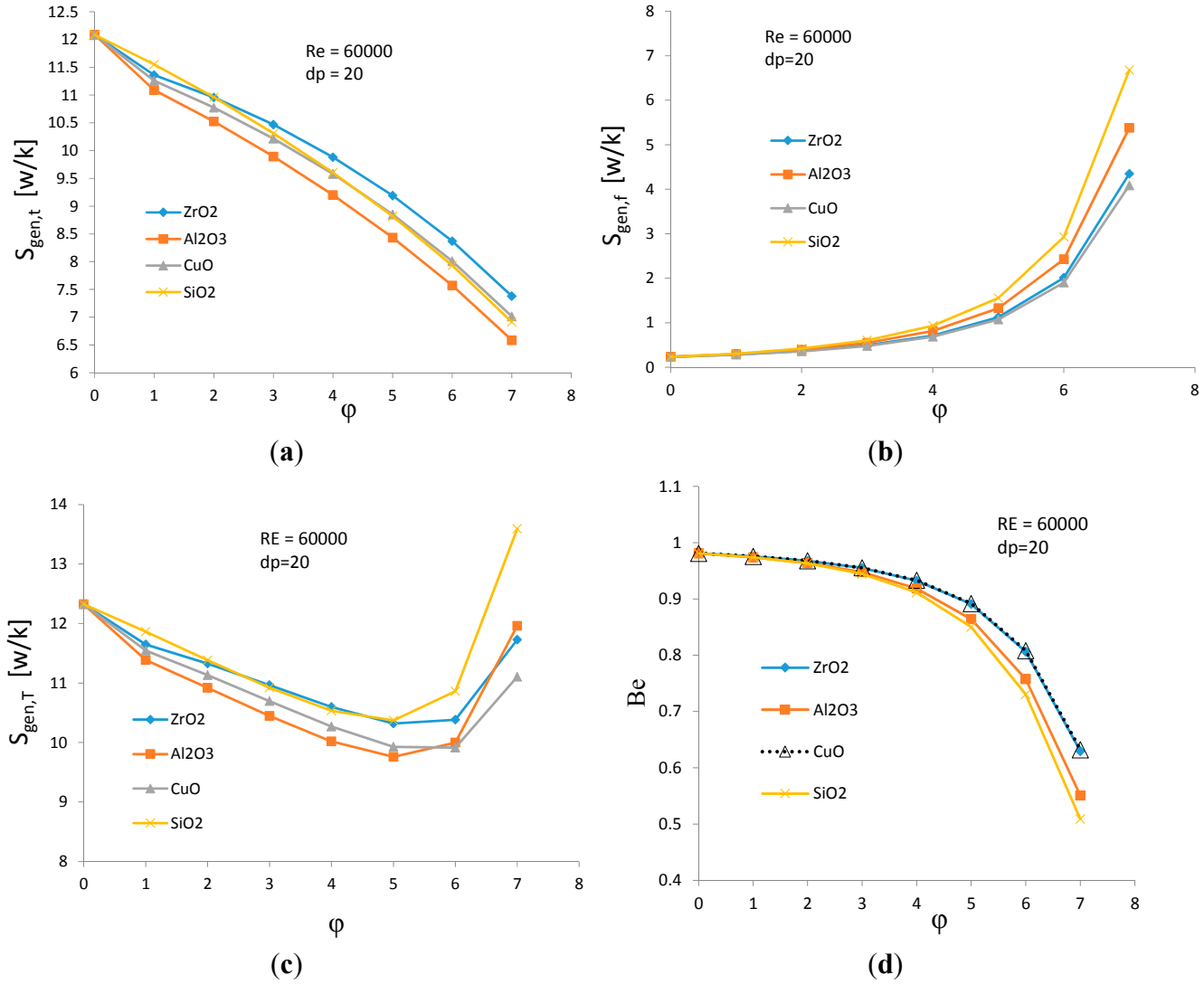

This study includes an analysis of the entropy generation of Al_2O_3-water and a comparison with nanofluids with other nanoparticles (ZrO_2, CuO, SiO_2). The present results for ZrO_2-water nanofluid were verified through a comparison with the results of Bianco *et al.* [36,37]. Figures 6a–d show that zirconia-water nanofluid used in the present study and Al_2O_3-water nanofluid used in references [36,37] exhibit a trend of variation similar to the variation trend of the volume fraction of nanoparticles as

well as Reynolds number and diameter of the particles. However, as discussed earlier the entropy generations for ZrO_2-water were generally more than those for Al_2O_3-water nanofluid.

4. Conclusions

In this paper the second law analysis of turbulent forced convection of ZrO_2-water nanofluid flow at constant heat flux is performed. Based on the results presented, the following conclusions are drawn:

(1) At a constant Reynolds number and for a given nanoparticle size, the thermal entropy generation decreases with the increase of concentration, while the frictional entropy generation has an opposite trend. The total entropy generation decreases to a minimum at 6% solid volume fraction and then increases with further increase of volume concentration.
(2) With an increase in Reynolds number, the total and the thermal entropy generation decrease, while the frictional entropy generation increases. The optimal volume concentration for minimum entropy generation decreases with the increase in Reynolds number.
(3) As nanoparticle size increases, the thermal and the total entropy generation increase, but the frictional entropy production decreases. The optimal concentration for minimum total entropy generation becomes higher for larger nanoparticle diameters.
(4) Al_2O_3-water nanofluid has the lowest thermal entropy generation, and the ZrO_2-water nanofluid has the highest. In terms of total entropy generation, the SiO_2-water nanofluid generated the highest entropy generation among the tested nanofluids.

Acknowledgments

The authors gratefully acknowledge UMRG Grant RP012A-13AET and High Impact Research Grant UM.C/625/1/HIR/MOHE/ENG/45, Faculty of Engineering, University of Malaya, Malaysia for support to conduct this research work.

Nomenclature

A:	Area (m^2)
Be:	Bejan number
Cp:	Specific heat (kJ $kg^{-1}\cdot K^{-1}$)
D:	Tube diameter (m)
dp:	Particle diameter (nm)
f:	Friction factor
k:	Thermal conductivity (Wm^{-1} K^{-1})
L:	Tube length (m)
Nu:	Nusselt number
m:	Mass flow rate (kg s^{-1})
p:	Pressure (Pa)
P:	Perimeter (m)
Pr:	Prandtl number, (μ Cp/k)
q:	Heat flux (Wm^{-2})
q':	Heat transfer per unit of length (Wm^{-1})
Re:	Reynolds number

Sgen:	Entropy generation (WK^{-1})
T:	Temperature (K)
x:	Axial coordinate (m)
V:	Velocity (ms^{-1}).
Greek Symbols	
φ:	Particles concentration
μ:	Dynamic viscosity (Nsm^{-2})
ρ:	Density (kgm^{-3}).
Subscripts	
Ave:	Average
bf:	Base fluid
d:	Nanoparticle diameter
eff:	Effective
f:	Frictional
g:	Generation
h:	Hydraulic
in:	Inlet
nf:	Nanofluids
out:	Outlet
p:	Particles
t:	Thermal
T:	Total

Author Contributions

The manuscript was written using the contributions of all the authors. All authors have read and approved the final manuscript.

Conflicts of Interest

The authors declare no conflict of interest

References

1. Maxwell, J.C. *A Treatise on Electricity and Magnetism*; Clarendon press: Oxford, UK, 1881; Volume 1.
2. Choi, S. Enhancing thermal conductivity of fluids with nanoparticles. In *Developments and Applications of Nonnewtonian Flows*; American Society of Mechanical Engineers: New York, NY, USA, 1995; pp. 99–106.
3. Mahian, O.; Kianifar, A.; Kleinstreuer, C.; Al-Nimr, M.A.; Pop, I.; Sahin, A.Z.; Wongwises, S. A review of entropy generation in nanofluid flow. *Int. J. Heat Mass Transf.* **2013**, *65*, 514–532.
4. Duangthongsuk, W.; Wongwises, S. Heat transfer enhancement and pressure drop characteristics of TiO_2—Water nanofluid in a double-tube counter flow heat exchanger. *Int. J. Heat Mass Transf.* **2009**, *52*, 2059–2067.
5. Huminic, G.; Huminic, A. Heat transfer characteristics in double tube helical heat exchangers using nanofluids. *Int. J. Heat Mass Transf.* **2011**, *54*, 4280–4287.

6. Duangthongsuk, W.; Selim Dalkilic, A.; Wongwises, S. Convective heat transfer of Al_2O_3-water nanofluids in a microchannel heat sink. *Curr. Nanosci.* **2012**, *8*, 317–322.
7. Li, J.; Kleinstreuer, C. Thermal performance of nanofluid flow in microchannels. *Int. J. Heat Fluid Flow* **2008**, *29*, 1221–1232.
8. Li, J.; Kleinstreuer, C. Microfluidics analysis of nanoparticle mixing in a microchannel system. *Microfluid. Nanofluidics* **2009**, *6*, 661–668.
9. Liu, Z.-H.; Li, Y.-Y. A new frontier of nanofluid research—application of nanofluids in heat pipes. *Int. J. Heat Mass Transf.* **2012**, *55*, 6786–6797.
10. Mohammadi, M.; Mohammadi, M.; Shafii, M. Experimental investigation of a pulsating heat pipe using ferrofluid (magnetic nanofluid). *J. Heat Transf.* **2012**, *134*, 014504.
11. Alizad, K.; Vafai, K.; Shafahi, M. Thermal performance and operational attributes of the startup characteristics of flat-shaped heat pipes using nanofluids. *Int. J. Heat Mass Transf.* **2012**, *55*, 140–155.
12. Shafahi, M.; Bianco, V.; Vafai, K.; Manca, O. An investigation of the thermal performance of cylindrical heat pipes using nanofluids. *Int. J. Heat Mass Transf.* **2010**, *53*, 376–383.
13. Shafahi, M.; Bianco, V.; Vafai, K.; Manca, O. Thermal performance of flat-shaped heat pipes using nanofluids. *Int. J. Heat Mass Transf.* **2010**, *53*, 1438–1445.
14. Yousefi, T.; Shojaeizadeh, E.; Veysi, F.; Zinadini, S. An experimental investigation on the effect of pH variation of MWCNT-H_2O nanofluid on the efficiency of a flat-plate solar collector. *Sol. Energy* **2012**, *86*, 771–779.
15. Gharehkhani, S.; Nouri-Borujerdi, A.; Kazi, S.N.; Yarmand, H. Extension of weighted sum of gray gas data to mathematical simulation of radiative heat transfer in a boiler with gas-soot media. *Sci. World J.* **2014**, *2014*, 504601.
16. Kulkarni, D.P.; Das, D.K.; Chukwu, G.A. Temperature dependent rheological property of copper oxide nanoparticles suspension (nanofluid). *J. Nanosci. Nanotechnol.* **2006**, *6*, 1150–1154.
17. Liu, M.-S.; Lin, M.C.-C.; Tsai, C.; Wang, C.-C. Enhancement of thermal conductivity with Cu for nanofluids using chemical reduction method. *Int. J. Heat Mass Transf.* **2006**, *49*, 3028–3033.
18. Haghshenas Fard, M.; Esfahany, M.N.; Talaie, M. Numerical study of convective heat transfer of nanofluids in a circular tube two-phase model *versus* single-phase model. *Int. Commun. Heat Mass Transf.* **2010**, *37*, 91–97.
19. Mahmoudi, A.H.; Shahi, M.; Raouf, A.H.; Ghasemian, A. Numerical study of natural convection cooling of horizontal heat source mounted in a square cavity filled with nanofluid. *Int. Commun. Heat Mass Transf.* **2010**, *37*, 1135–1141.
20. Yoo, D.-H.; Hong, K.; Yang, H.-S. Study of thermal conductivity of nanofluids for the application of heat transfer fluids. *Thermochim. Acta* **2007**, *455*, 66–69.
21. Xie, H.; Wang, J.; Xi, T.; Liu, Y.; Ai, F.; Wu, Q. Thermal conductivity enhancement of suspensions containing nanosized alumina particles. *J. Appl. Phys.* **2002**, *91*, 4568–4572.
22. Maïga, S.E.B.; Nguyen, C.T.; Galanis, N.; Roy, G.; Maré, T.; Coqueux, M. Heat transfer enhancement in turbulent tube flow using Al_2O_3 nanoparticle suspension. *Int. J. Numer. Methods Heat Fluid Flow* **2006**, *16*, 275–292.

23. Vajjha, R.S.; Das, D.K.; Kulkarni, D.P. Development of new correlations for convective heat transfer and friction factor in turbulent regime for nanofluids. *Int. J. Heat Mass Transf.* **2010**, *53*, 4607–4618.
24. Yarmand, H.; Gharehkhani, S.; Kazi, S.N.; Sadeghinezhad, E.; Safaei, M.R. Numerical investigation of heat transfer enhancement in a rectangular heated pipe for turbulent nanofluid. *Sci. World J.* **2014**, *2014*, doi:10.1155/2014/369593.
25. Mahian, O.; Mahmud, S.; Pop, I. Analysis of first and second laws of thermodynamics between two isothermal cylinders with relative rotation in the presence of MHD flow. *Int. J. Heat Mass Transf.* **2012**, *55*, 4808–4816.
26. Bejan, A. *Entropy Generation Minimization: The Method of Thermodynamic Optimization of Finite-size Systems and Finite-time Processes*; CRC Press: New York, NY, USA, 1995.
27. Oztop, H.F.; Al-Salem, K. A review on entropy generation in natural and mixed convection heat transfer for energy systems. *Renew. Sustain. Energy Rev.* **2012**, *16*, 911–920.
28. Şahin, A.Z. Entropy generation in turbulent liquid flow through a smooth duct subjected to constant wall temperature. *Int. J. Heat Mass Transf.* **2000**, *43*, 1469–1478.
29. Mahian, O.; Mahmud, S.; Heris, S.Z. Analysis of entropy generation between co-rotating cylinders using nanofluids. *Energy* **2012**, *44*, 438–446.
30. Mahian, O.; Mahmud, S.; Heris, S.Z. Effect of uncertainties in physical properties on entropy generation between two rotating cylinders with nanofluids. *J. Heat Transf.* **2012**, *134*, 101704.
31. Ko, T.; Ting, K. Entropy generation and optimal analysis for laminar forced convection in curved rectangular ducts: A numerical study. *Int. J. Therm. Sci.* **2006**, *45*, 138–150.
32. Leong, K.; Saidur, R.; Mahlia, T.; Yau, Y. Entropy generation analysis of nanofluid flow in a circular tube subjected to constant wall temperature. *Int. Commun. Heat Mass Transf.* **2012**, *39*, 1169–1175.
33. Bianco, V.; Manca, O.; Nardini, S. Second law analysis of-water nanofluid turbulent forced convection in a circular cross section tube with constant wall temperature. *Adv. Mech. Eng.* **2013**, *2013*, doi:10.1155/2013/920278.
34. Moghaddami, M.; Mohammadzade, A.; Esfehani, S.A.V. Second law analysis of nanofluid flow. *Energy Convers. Manag.* **2011**, *52*, 1397–1405.
35. Moghaddami, M.; Shahidi, S.; Siavashi, M. Entropy generation analysis of nanofluid flow in turbulent and laminar regimes. *J. Comput. Theor. Nanosci.* **2012**, *9*, 1586–1595.
36. Bianco, V.; Nardini, S.; Manca, O. Enhancement of heat transfer and entropy generation analysis of nanofluids turbulent convection flow in square section tubes. *Nanoscale Res. Lett.* **2011**, *6*, 1–12.
37. Bianco, V.; Manca, O.; Nardini, S. Entropy generation analysis of turbulent convection flow of Al_2O_3–water nanofluid in a circular tube subjected to constant wall heat flux. *Energy Convers. Manag.* **2014**, *77*, 306–314.
38. Das, S.K.; Putra, N.; Thiesen, P.; Roetzel, W. Temperature dependence of thermal conductivity enhancement for nanofluids. *J. Heat Transf.* **2003**, *125*, 567–574.
39. Hoffmann, K.A.; Chiang, S.T. *Computational Fluid Dynamics*, Volume 1; Wichita, K.S., Ed.; Engineering Education System: Washington, DC, USA, 2000.

40. Corcione, M. Heat transfer features of buoyancy-driven nanofluids inside rectangular enclosures differentially heated at the sidewalls. *Int. J. Therm. Sci.* **2010**, *49*, 1536–1546.
41. Ratts, E.B.; Raut, A.G. Entropy generation minimization of fully developed internal flow with constant heat flux. *J. Heat Transf.* **2004**, *126*, 656–659.
42. Pak, B.C.; Cho, Y.I. Hydrodynamic and heat transfer study of dispersed fluids with submicron metallic oxide particles. *Exp. Heat Transf. Int. J.* **1998**, *11*, 151–170.
43. Williams, W.; Hu, L.-W.; Buongiorno, J. Experimental investigation of turbulent convective heat transfer and pressure loss of alumina/water and zirconia/water nanoparticle colloids (nanofluids) in horizontal tubes. *J. Heat Transf.* **2008**, *130*, 1–7.
44. Teng, T.-P.; Hung, Y.-H.; Teng, T.-C.; Mo, H.-E.; Hsu, H.-G. The effect of alumina/water nanofluid particle size on thermal conductivity. *Appl. Therm. Eng.* **2010**, *30*, 2213–2218.
45. Kleinstreuer, C.; Feng, Y. Experimental and theoretical studies of nanofluid thermal conductivity enhancement: A review. *Nanoscale Res. Lett.* **2011**, *6*, 1–13.